Solid-State Electronics, 1976, Vol. 19, pp. 739–744. Pergamon Press. Printed in Great Britain

ANALYTICAL SOLUTIONS FOR THE BREAKDOWN VOLTAGE OF ABRUPT CYLINDRICAL AND SPHERICAL JUNCTIONS

B. JAYANT BALIGA
General Electric Corporate Research and Development Center, Schenectady, NY 12301, U.S.A.

and

SORAB K. GHANDHI
Electrical and Systems Engineering Department, Rensselaer Polytechnic Institute, Troy, NY 12181, U.S.A.

(*Received* 11 *December* 1975; *in revised form* 28 *February* 1976)

Abstract—Analytical solutions for the breakdown voltage of abrupt cylindrical and spherical junctions have been obtained, using suitable approximations for the electric field in the depletion layer. These solutions are shown to be within ± 1% of exact computer solutions for doping densities of less than 10^{16} cm^{-3}. By normalization to the parallel plane case, these solutions have been presented in a form which allows the computation of the breakdown voltage of both cylindrical and spherical junctions using a single curve for each situation.

INTRODUCTION

Modern integrated circuit technology is based on the feasibility of making a large number of separate *p-n* junctions on a single substrate. Such junctions are conventionally fabricated by diffusion of impurities, through a photolithographically delineated window in an impervious masking layer, to form a "planar" junction in the substrate material. For a rectangular window, such a junction consists of a plane structure terminated with cylindrical curved boundaries at the window edge. In addition, if the window has sharp corners, the junction contains a spherical boundary at these locations. It has been shown that the breakdown voltage of a planar junction is limited by avalanche multiplication at these curved junction boundaries, rather than in the parallel plane portion of the junction. Analyses of both cylindrical and spherical abrupt junctions, using computerized solutions of the ionization integral, have resulted in a set of design curves relating the breakdown voltage to the radius of curvature and the doping concentration in the substrate[1, 2]. These theoretical results have been experimentally verified[3, 4]. Computations have also been extended to the case of diffused junctions by taking into account the voltage supported in the diffused portion of the junction[5–10].

Solution for the breakdown voltage requires the calculation of the ionization integral for a two-dimensional situation. The general approach[9, 10] is to solve this integral along various paths followed by avalanching hole-electron pairs. The path of maximum multiplication is usually the electrical field line which passes through the point of maximum electric field. Solution along this path gives the breakdown voltage.

This paper provides analytical solutions for the breakdown voltage of both cylindrical and spherical abrupt planar junctions by the use of suitable approximations for the field distribution in these junctions. Although based on the simple one-dimensional approach of integration along a radius vector, the solutions are reasonably close to computer derived values for all practical purposes. This approach allows the condensation of the multiplicity of curves provided in the literature into a single curve, and can be used for the calculation of the break-down voltage of planar junctions with any given radius of curvature and background doping density.

PARALLEL PLANE JUNCTION

This section considers the breakdown of parallel plane junctions. Quantities derived here will be used subsequently to provide normalized solutions to the breakdown voltage of the curved junctions. In the parallel plane case, Poisson's equation using the depletion layer approximation can be written as

$$\frac{d^2V}{dx^2} = -\frac{dE}{dx} = -\frac{qN_B}{\epsilon\epsilon_0} \tag{1}$$

where V is the applied voltage, E is the electric field, q is the electronic charge, N_B is the background doping $(N_D - N_A)$, ϵ is the relative permittivity, and ϵ_0 is the dielectric constant of free space. Solving for the electric field and voltage distribution at breakdown[11]:

$$E = \frac{qN_B}{\epsilon\epsilon_0}(x - W_c) \tag{2}$$

$$V = \frac{qN_B}{2\epsilon\epsilon_0}(2W_c x - x^2) \tag{3}$$

where W_c is the depletion layer width at breakdown for the parallel plane junction.

Sze and Gibbons[1] have used separate values for the ionization coefficients of electrons and holes, as provided by Lee *et al.*[12], in their computations of the breakdown voltage. These computations can be greatly simplified by using the concept of an average ionization coefficient.

固态电子学。1976年。第19卷。第739-744页。Pergamon Press。英国印刷

用于突发圆柱形和球形连接器的电压断裂的解析解

B. Jayant Baliga
通用电气公司企业研发中心，纽约州斯克内克塔迪，12301，美国

SORAB K. GHANDHI
电气与系统工程系，伦斯勒理工学院，纽约州特洛伊，12181，美国

(收到日期：1975年12月11日；修改稿收到日期：1976年2月28日)

摘要--利用适用于耗尽层电场的合适近似，已获得陡峭圆柱形和球形结击穿电压的解析解。这些解被证明在掺杂浓度小于10 a6 cm ~时，与精确的计算机解的误差在 -+1% 以内。通过归一化到平行平面情况，这些解以允许使用每种情况的单个曲线来计算圆柱形和球形结击穿电压的形式呈现。

引言

现代集成电路技术基于在单个衬底上制作大量独立p-n结的可行性。此类结通常通过在不可渗透的掩模层中的光刻图形化窗口扩散杂质来制造，在衬底材料中形成“平面”结。对于矩形窗口，此类结由在窗口边缘以圆柱形弯曲边界终止的平面结构组成。此外，如果窗口有尖锐的角，结在这些位置包含球形边界。研究表明，平面结的击穿电压受限于这些弯曲结边界处的雪崩倍增，而不是结的平行平面部分的雪崩倍增。使用离子化积分的计算机解对圆柱形和球形陡峭结的分析，得出了一套将击穿电压与曲率半径和衬底掺杂浓度相关的设计曲线1, 2。这些理论结果已通过实验验证3,4。计算还扩展到了扩散结的情况，考虑了扩散部分所支持的电压5-10。

求解击穿电压需要计算二维情况下的电离积分。通常的方法9, 10是沿着不同路径求解该积分，这些路径是雪崩倍增的空穴-电子对所遵循的。最大倍增的路径通常是穿过最大电场点的电场线。沿着该路径的求解可以得到击穿电压。

本文通过使用适用于这些结中场分布的合适近似，为圆柱形和球形突变平面结的击穿电压提供了解析解。尽管基于沿半径向量的简单一维方法，但这些解在实际应用中与计算机计算值相当接近。这种方法可以将文献中提供的多种曲线浓缩为一条曲线，并且可用于计算具有任何给定曲率半径和背景掺杂密度的平面结的击穿电压。

本文通过使用适用于这些结中场分布的合适近似，为圆柱形和球形突变平面结的击穿电压提供了解析解。尽管基于沿半径向量的简单一维方法，但这些解在实际应用中与计算机计算值相当接近。这种方法可以将文献中提供的多种曲线浓缩为一条曲线，并且可用于计算具有任何给定曲率半径和背景掺杂密度的平面结的击穿电压。

平行平面结

本节考虑平行平面结的击穿。此处推导出的量将随后用于为弯曲结的击穿电压提供归一化解。在平行平面情况下，使用耗尽层近似泊松方程可以写为

$$\frac{d2V}{dx:} = \frac{dE}{dx} = \frac{qNR}{e6o} \tag{1}$$

其中V是施加电压，E是电场，q是电子电荷，N8是背景掺杂*(No- NA)*, 6是相对介电常数，ε0是自由空间的介电常数。求解击穿l 1时的电场和电压分布：

$$E = \frac{qN_B}{\epsilon\epsilon_0}(x - W_c)$$

$$V = \frac{qN_B}{2\epsilon\epsilon_0}(2W_c x - x^2)$$

其中 Wc 是平行平面结在击穿时的耗尽层宽度。

Sze 和 Gibbonsl 在计算击穿电压时，使用了分别针对电子和空穴的离化系数，这些系数来自 Lee 等人 12 的研究。通过使用平均离化系数的概念，这些计算可以大大简化。

Using this concept, the breakdown voltage can be obtained by solving the ionization integral:

$$\int_0^{W_c} \alpha \, dx = 1. \tag{4}$$

In this paper a simple approximation to the dependence of the average ionization coefficient upon electric field for silicon, given by Fulop[13], is used:

$$\alpha = AE^7 \text{ cm}^{-1} \tag{5}$$

where

$$A = 1.8 \times 10^{-35}. \tag{6}$$

Combining with (2) and (4), the depletion layer width at breakdown for the parallel plane case is obtained as

$$W_c = \left(\frac{8}{A}\right)^{1/8} \left(\frac{\epsilon\epsilon_0}{qN_B}\right)^{7/8} \tag{7}$$

and the corresponding peak electric field as

$$E_{pPP} = \left(\frac{8}{A} \cdot \frac{qN_B}{\epsilon\epsilon_0}\right)^{1/8} = \left(\frac{8}{AW_c}\right)^{1/7}. \tag{8}$$

After making the necessary numerical substitutions for silicon,

$$E_{pPP} = 4010\, N_B^{1/8} \text{ V/cm}. \tag{9}$$

This result is in excellent agreement (within ± 1%) with the values derived by Sze and Gibbons[1], for doping densities under 1×10^{16} cm^{-3}.

Further, substitution of numerical values for silicon into (7) and (3) gives

$$W_c = 2.67 \times 10^{10}\, N_B^{-7/8} \tag{10}$$

and the breakdown voltage as

$$BV_{PP} = 6.40 \times 10^{13}\, N_B^{-3/4} \tag{11}$$

which are also in excellent agreement with[1]. From this we conclude that Fulop's formula for the ionization coefficient can be successfully used to calculate breakdown voltages for doping levels below 1×10^{16} cm^{-3}. Therefore, this form has been used in subsequent sections.

CYLINDRICAL JUNCTION

Poisson's equation for the voltage distribution in the depletion layer of a cylindrical junction can be written as

$$\frac{1}{r}\frac{d}{dr}\left(r\frac{dV}{dr}\right) = -\frac{1}{r}\frac{d}{dr}(rE) = -\left(\frac{qN_B}{\epsilon\epsilon_0}\right) \tag{12}$$

Solving for the electric field and voltage distributions gives

$$E = \frac{qN_B}{2\epsilon\epsilon_0}\left(\frac{r^2 - r_d^2}{r}\right) \tag{13}$$

and

$$V = \frac{qN_B}{2\epsilon\epsilon_0}\left[\left(\frac{r_j^2 - r^2}{2}\right) + r_d^2 \ln\left(\frac{r}{r_j}\right)\right] \tag{14}$$

where r_j is the radius of curvature of the metallurgical junction and r_d is the radius of curvature of the depletion layer boundary.

Again, the peak electric field at breakdown can be determined by using the field distribution (13) to solve the ionization integral, but this expression does not allow a simple direct solution. However, the seventh power law dependence of the ionization coefficient upon electric field results in most of the ionization being confined to the high field regions of the junction depletion layer. Examination of (13) shows that, for cylindrical junctions, this region is largely confined to small values of r near the boundary of the metallurgical junction. This allows an approximation to (13),

$$E = \frac{K}{r} \tag{15}$$

for substitution in the ionization integral. This hyperbolic approximation for the electric field results in the "depletion layer" extending to infinity. Thus the ionization integral must be performed from the metallurgical junction boundary, r_j, to infinity. Carrying out this integration, the peak electric field at breakdown is obtained as

$$E_{pC} = \left(\frac{6}{Ar_j}\right)^{1/7}. \tag{16}$$

Normalizing to the parallel plane case,

$$\frac{E_{pC}}{E_{pPP}} = \left(\frac{3W_c}{4r_j}\right)^{1/7} \simeq \left(\frac{W_c}{r_j}\right)^{1/7}. \tag{17}$$

Typical data for the peak electric field of cylindrical junctions, taken from Fig. 12 of [1], is listed in Table 1 for

Table 1. Peak electric field at breakdown for cylindrical junctions taken from Ref. [1]

Doping N_B (cm^{-3})	E_{pPP} (V/cm)	r_j (microns)	E_{pC} (V/cm)	W_c (microns)	$\frac{W_c}{r_j}$	$\frac{E_{pC}}{E_{pPP}}$
1×10^{14}	2.3×10^5	10	3.3×10^5	150	15	1.44
		5	3.7		30	1.61
		1	4.7		150	2.04
		0.5	5.4		300	2.35
2×10^{14}	2.6×10^5	10	3.4×10^5	80	8	1.31
		5	3.7		16	1.42
		1	4.7		80	1.81
		0.5	5.4		160	2.08
5×10^{14}	2.9×10^5	10	3.4×10^5	35	3.5	1.17
		5	3.7		7	1.28
		1	4.7		35	1.62
		0.5	5.4		70	1.86
1×10^{15}	3.15×10^5	10	3.5×10^5	18	1.8	1.11
		5	3.8		3.6	1.21
		1	4.7		18	1.49
		0.5	5.4		36	1.71
2×10^{15}	3.4×10^5	10	3.6×10^5	10	1	1.06
		5	3.9		2	1.15
		1	4.8		10	1.41
		0.5	5.4		20	1.59
5×10^{15}	3.8×10^5	1	4.9×10^5	4.7	4.7	1.29
		0.5	5.5		9.4	1.45
1×10^{16}	4.1×10^5	1	5×10^5	2.5	2.5	1.22
		0.5	5.5		5.0	1.34

利用这一概念，可以通过求解离化积分来获得击穿电压。

$$\int_0^{W_c} \alpha \, dx = 1.$$

在本文中，使用了Fulop13给出的硅中平均电离系数对电场依赖关系的简单近似式：

其中

结合(2)和(4)，平行平面情况下的击穿耗尽层宽度得到

$$W_c = \left(\frac{8}{A}\right)^{1/8} \left(\frac{\epsilon\epsilon_0}{qN_B}\right)^{7/8}$$

以及相应的峰值电场为

$$E_{pPP} = \left(\frac{8}{A} \cdot \frac{qN_B}{\epsilon\epsilon_0}\right)^{1/8} = \left(\frac{8}{AW_c}\right)^{1/7}.$$

在硅中进行必要的数值代入后，

$$E_{pPP} = 4010\, N_B^{1/8} \text{ V/cm}.$$

此结果与Sze和Gibbonsl推导的值（在+-1%以内）完全一致，适用于掺杂浓度低于 **1x 10'6cm 3**的情况。

此外，将硅的数值代入(7)和(3)中，得到

$$W_c = 2.67 \times 10^{10}\, N_B^{-7/8}$$

以及击穿电压为

$$BV_{PP} = 6.40 \times 10^{13}\, N_B^{-3/4}$$

这些也与1高度一致。由此我们得出结论，Fulop的离子化系数公式可以成功用于计算掺杂水平低于 **1x 1016cm 3**的击穿电压。因此，本节后续部分采用了这种形式。

圆柱形结

圆柱形结耗尽层中的电压分布泊松方程可以表示为

$$\frac{1}{r}\frac{d}{dr}\left(r\frac{dV}{dr}\right) = -\frac{1}{r}\frac{d}{dr}(rE) = -\left(\frac{qN_B}{\epsilon\epsilon_0}\right) \qquad (12)$$

求解电场和电压分布可以得到

$$E = \frac{qN_B}{2\epsilon\epsilon_0}\left(\frac{r^2 - r_d^2}{r}\right)$$

$$V = \frac{qN_B}{2\epsilon\epsilon_0}\left[\left(\frac{r_j^2 - r^2}{2}\right) + r_d^2 \ln\left(\frac{r}{r_j}\right)\right]$$

其中rj是金属结的曲率半径，ra是耗尽层边界的曲率半径。

再次，击穿时的峰值电场可以通过使用场分布（13）来求解电离积分来确定，但该表达式不允许

电离系数对电场的七次方依赖关系导致大部分电离被限制在结耗尽层的高电场区域。检查(13)式表明，对于圆柱形结，该区域主要被限制在靠近金属结边界的小r值附近。这允许对(13)式进行近似，

结耗尽层的场区。对(13)的检查表明，对于圆柱形结，该区域主要局限于靠近冶金结边界处r的小值。这允许对(13)进行近似，

$$E = \frac{K}{r}$$

用于电离积分的代入。这种对电场的双曲线近似导致"耗尽层"延伸至无穷远。因此，电离积分必须从结边界、r~到无穷远进行。积分中，获得的峰值电场为

在击穿条件下进行金属化处理是

$$E_{pC} = \left(\frac{6}{Ar_j}\right)^{1/7}.$$

将其归一化到平行平面情况，

$$\frac{E_{pC}}{E_{pPP}} = \left(\frac{3W_c}{4r_j}\right)^{1/7} \simeq \left(\frac{W_c}{r_j}\right)^{1/7}.$$

圆柱形结的峰值电场典型数据，取自文献1的图12，列于表I中

表1. 参照文献1中圆柱形结击穿时的峰值电场~

ng	E_{pPP} (V/cm)	r_j (microns)			$\frac{E_{pC}}{E_{pPP}}$
1 x IO 14	2.3 x IO 5		3.3 x Io-		1.44
					1.61
					2.04
					2.35
2 x 1014	2.6 x Io 5		3.4 x Io-		1.31
					1.42
					1.81
					2.08
5 x 1014	2.9 x ~o 5		3.4 x IO*		1.17
			I 3,7		1.28
					1.62
					1.86
1 x i0 1)-	3.15 x ifr		3,5 x i0*		1.11
					1.21
					1.49
					1.71
2 x IO I~	3,4 x Io 5		3.6 x io*		1.06
					1.15
		1			1.41
					1.59
5 x IO 15	3,8 x Io 5		2-, 9 x 10 5		1.29
					1.45
1 x Io 16	4. I x Io 5		5 x 10 5		1.22
					1.34

background doping densities less than $1 \times 10^{16}\,cm^{-3}$, and compared with the analytical solution (17) in Fig. 1. Good agreement between the two solutions is observed for doping densities below $1 \times 10^{16}\,cm^{-3}$ and for (W_c/r_j) ratios greater than unity.

Using the above relationship between the peak electric field in the cylindrical and parallel plane cases, it is possible to normalize the breakdown voltage of an abrupt cylindrical junction to the corresponding (same background doping) parallel plane junction, Using (3) and (14), this ratio can be derived:

$$\frac{BV_C}{BV_{PP}} = \frac{2}{W_c E_{pPP}}\left[\frac{E_{pC} r_j}{2} + \frac{1}{2}\left(\frac{qN_B}{2\epsilon\epsilon_0} r_j^2 - E_{pC} r_j\right) \cdot \ln\left(1 - \frac{2\epsilon\epsilon_0 E_{pC}}{qN_B r_j}\right)\right] \quad (18)$$

which reduces to

$$\frac{BV_C}{BV_{PP}} = \left\{\frac{1}{2}\left[\left(\frac{r_j}{W_c}\right)^2 + 2\left(\frac{r_j}{W_c}\right)^{6/7}\right] \cdot \ln\left[1 + 2\left(\frac{W_c}{r_j}\right)^{8/7}\right] - \left(\frac{r_j}{W_c}\right)^{6/7}\right\} \quad (19)$$

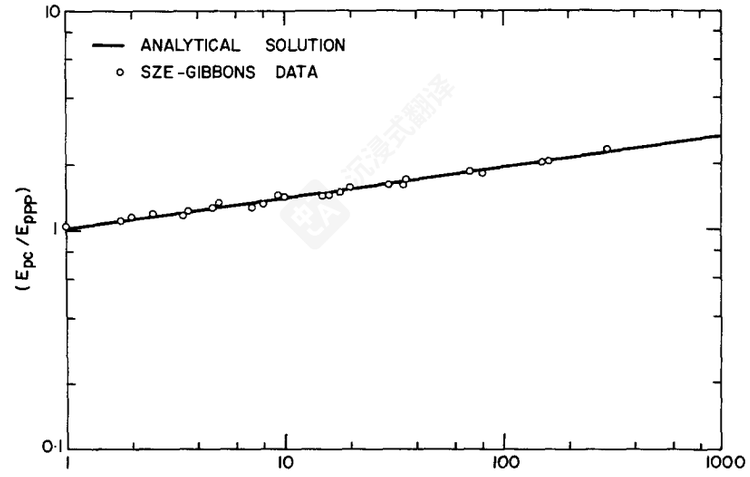

Fig. 1. Comparison of normalized peak electric fields in the analytical case with computer-derived solutions of [1] for cylindrical junctions.

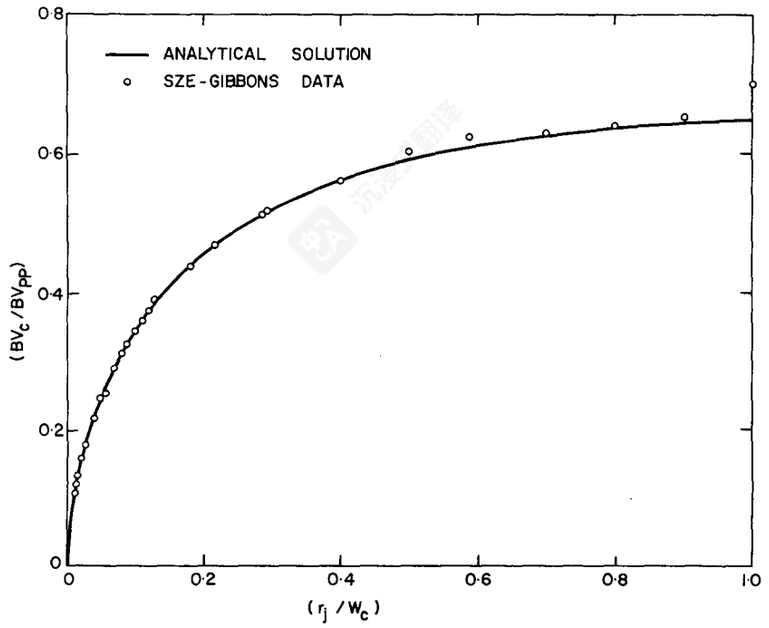

Fig. 2. Comparison of normalized breakdown voltage in the analytical case with computer-derived solutions of [1] for cylindrical junctions.

背景掺杂密度小于 1× 10z6cm-3，并与图1中的解析解(17)进行比较。对于掺杂密度低于1× 10-6cm-3以及(W,/ri)比值大于1的情况，两种解法吻合良好。

利用上述圆柱形结与平行平面情况下的峰值电场关系，可以将陡峭圆柱形结的击穿电压归一化到相应的（相同背底掺杂）平行平面结，使用（3）和（14），可以推导出该比值：

$$\frac{BV_C}{BV_{PP}} = \frac{2}{W_c E_{pPP}}\left[\frac{E_{pC} r_j}{2} + \frac{1}{2}\left(\frac{qN_B}{2\epsilon\epsilon_0} r_j^2 - E_{pC} r_j\right) \cdot \ln\left(1 - \frac{2\epsilon\epsilon_0 E_{pC}}{qN_B r_j}\right)\right]$$

简化为

$$\frac{BV_C}{BV_{PP}} = \left\{\frac{1}{2}\left[\left(\frac{r_j}{W_c}\right)^2 + 2\left(\frac{r_j}{W_c}\right)^{6/7}\right] \cdot \ln\left[1 + 2\left(\frac{W_c}{r_j}\right)^{8/7}\right] - \left(\frac{r_j}{W_c}\right)^{6/7}\right\},$$

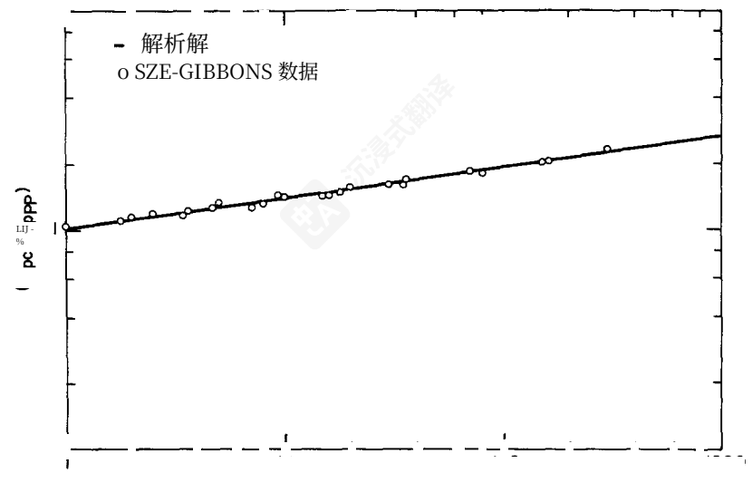

图 I. 解析解中归一化峰值电场与圆柱形结计算机求解结果的比较。

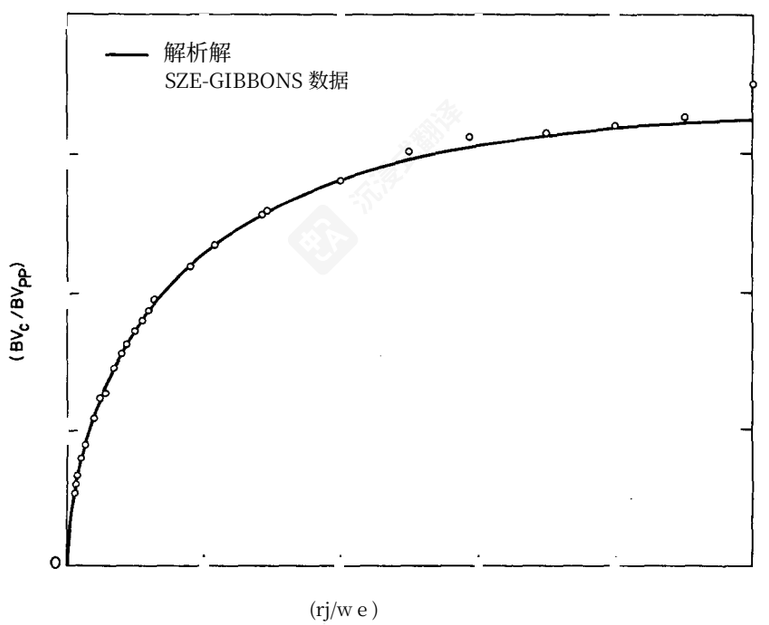

图 2. 解析解中归一化击穿电压与圆柱形结计算机求解的 l 对比。

with the application of (17). This formulation for the breakdown voltage of cylindrical junctions is plotted in Fig. 2, and compared with examples taken from the computations of Sze and Gibbons (Table 2). The agreement between the analytical solution and the computer-derived solution is extremely good for values of (r_j/W_c) below 0.9.

SPHERICAL JUNCTIONS

In the case of spherical junctions, Poisson's equation for the depletion layer can be written as

$$\frac{1}{r^2}\frac{\mathrm{d}}{\mathrm{d}r}\left(r^2\frac{\mathrm{d}V}{\mathrm{d}r}\right) = -\frac{1}{r^2}\frac{\mathrm{d}}{\mathrm{d}r}(r^2E) = -\left(\frac{qN_B}{\epsilon\epsilon_0}\right). \quad (20)$$

Solving for the electric field and voltage distribution gives

$$E = \frac{qN_B}{3\epsilon\epsilon_0}\left(\frac{r^3 - r_d^3}{r^2}\right) \quad (21)$$

Table 2. Breakdown voltages of cylindrical junctions taken from Refs. [1 and 11]

Doping (cm^{-3})	W_c (microns)	BV_{pp} (V)	r_j (microns)	BV_c (V)	(r_j/W_c)	$V_{RC} = BV_c/BV_{pp}$
2×10^{14}	80	1200	1	130	0.0125	0.108
3×10^{15}	7.2	150	0.1	18	0.0139	0.120
3×10^{14}	55	820	1	110	0.0182	0.134
5×10^{15}	4.6	100	0.1	16	0.0217	0.160
5×10^{14}	34	540	1	96	0.0294	0.178
1×10^{16}	2.5	64	0.1	14	0.040	0.219
9×10^{14}	20	340	1	84	0.050	0.247
1×10^{15}	17	320	1	81	0.0588	0.253
1×10^{15}	17	320	1.2	93	0.0706	0.291
1×10^{15}	17	320	1.4	100	0.0824	0.3125
1×10^{15}	17	320	1.5	105	0.0882	0.325
1×10^{15}	17	320	1.7	110	0.100	0.344
1×10^{15}	17	320	1.9	115	0.112	0.359
1×10^{15}	17	320	2.0	120	0.118	0.375
1×10^{15}	17	320	2.2	125	0.129	0.391
3×10^{14}	55	820	10	360	0.182	0.439
5×10^{15}	4.6	100	1	47	0.217	0.470
7×10^{15}	3.5	82	1	42	0.286	0.512
5×10^{14}	34	540	10	280	0.294	0.519
1×10^{16}	2.5	64	1	36	0.400	0.5625
9×10^{14}	20	340	10	205	0.500	0.603
1×10^{15}	17	320	10	200	0.588	0.625
1.3×10^{15}	14.3	270	10	170	0.700	0.630
1.6×10^{15}	12.5	250	10	160	0.800	0.640
1.8×10^{15}	11.1	230	10	150	0.900	0.652
2×10^{15}	10	200	10	140	1.000	0.700

Table 3. Breakdown voltages of spherical junctions taken from Refs. [1 and 11]

Doping (cm^{-3})	W_c (microns)	BV_{PP} (V)	r_j (microns)	BV_S (V)	r_j/W_c	$V_{RS} = BV_S/BV_{PP}$
2×10^{14}	80	1200	1	47	0.0125	0.039
3×10^{14}	55	820	1	44	0.0182	0.0537
5×10^{14}	34	540	1	42	0.0294	0.078
7×10^{14}	25	420	1	40	0.040	0.095
1×10^{15}	17	320	1	40	0.0588	0.125
1×10^{14}	150	2000	10	260	0.0667	0.130
2×10^{15}	10	200	1	35	0.100	0.175
2×10^{14}	80	1200	10	240	0.125	0.200
3×10^{15}	7.2	150	1	33	0.139	0.220
3×10^{14}	55	820	10	210	0.182	0.256
5×10^{15}	4.6	100	1	30	0.217	0.300
7×10^{15}	3.5	82	1	27	0.286	0.329
5×10^{14}	34	540	10	180	0.294	0.333
1×10^{16}	2.5	64	1	25	0.400	0.391
7×10^{14}	25	420	10	160	0.400	0.381
9×10^{14}	12.5	250	10	150	0.500	0.429
1×10^{15}	17	320	10	145	0.588	0.453
1.3×10^{15}	14.3	270	10	130	0.700	0.481
1.6×10^{15}	12.5	250	10	125	0.800	0.500
1.8×10^{15}	11.1	230	10	120	0.900	0.522
2×10^{15}	10	200	10	105	1.000	0.525

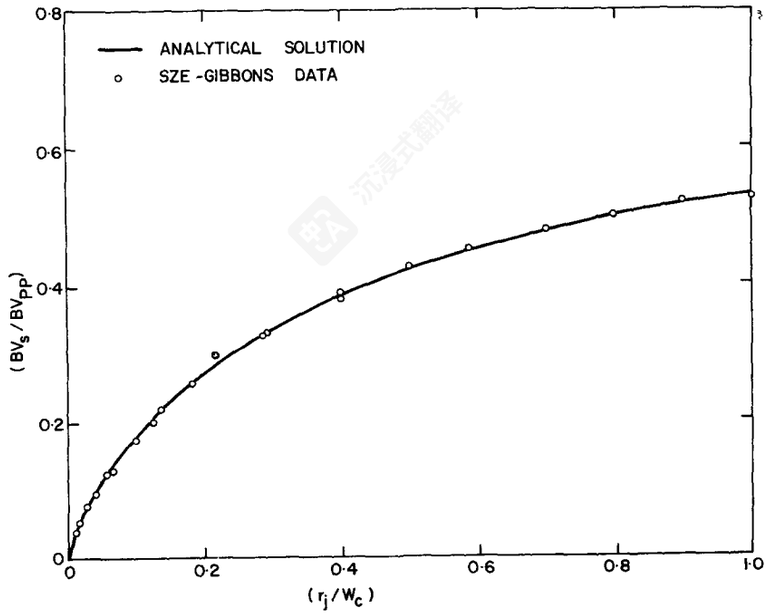

Fig. 3. Comparison of normalized breakdown voltage in the analytical case with computer-derived solutions of [1] for spherical junctions.

在应用(17)时。圆柱形结的击穿电压公式绘制在图2中，并与Sze和Gibbons的计算示例（表2）进行比较。对于(rJW,.)值低于0.9的情况，解析解与计算机求解结果的一致性非常好。

球形结
对于球形结，泊松方程

耗尽层的表达式可以写为

$$\frac{1}{r^2}\frac{\mathrm{d}}{\mathrm{d}r}\left(r^2\frac{\mathrm{d}V}{\mathrm{d}r}\right) = -\frac{1}{r^2}\frac{\mathrm{d}}{\mathrm{d}r}(r^2E) = -\left(\frac{qN_B}{\epsilon\epsilon_0}\right). \quad (20)$$

求解电场和电压分布得到

$$E = \frac{qN_B}{3\epsilon\epsilon_0}\left(\frac{r^3 - r_d^3}{r^2}\right) \quad (21)$$

表 2. 圆柱形结的击穿电压 参考文献 1 和 11

Doping (cm^{-3})	.cron-1 (V)	L (mio-oo-)	I (V)	$V_{RC} = BV_c/BV_{pp}$
2×10^{14}			130 ~ 0. 0125	
3×10^{15}			18 I 0.0139	
3×10^{14}			ii0 I O,Ol~	
5×10^{15}	l i00		16 l 0,0217	
5×10^{14}			I o.o29~	0.178
1×10^{16}			14 l 0.040	
9×10^{14}			~4 L 0.050	
1×10^{15}			81 I 0.0588	
1×10^{15}	I 320		93 i 0.0706	
1×10^{15}			i00 ~ 0,0824	
1×10^{15}			105 l 0.0-2	
1×10^{15}			iio I o.1oo	0,344
1×10^{15}	I 320		I15 I o.112	
1×10^{15}	L 320		12o I 0.//8	
1×10^{15}	I 320		125 I 0.129	
3×10^{14}	I 820		360 I 0.182	0.h39
5×10^{15}	I i00		47 I 0.217	
7×10^{15}			~ 0.2e-6	
5×10^{14}	I 540		280 I 0,294	0,519
1×10^{16}			36 l 0.40O	
9×10^{14}	i 340		I 205 I 0.500	
1×10^{15}	l 320		I 200 I 0.58-	
1.3×10^{15}	I 270		I 170 I 0.700	
1.6×10^{15}	I 250		l 160 I 0,800	
1.8×10^{15}	I 230		I 150 I 0.900	
2×10^{15}	I 200		lhO I I,CO0	0,700

表3. 从球形Ref. 1和11结中提取的击穿电压

掺杂 (~3)	(微米) (V)	(微米)			
2 x 10 lh					
3 x IO 14				o.o182	o.o531
5 x Io 14				0,0-9~	0,078
7 x IO 14				o.oho	0,095
1 x 1015					0,,25
I x IO Il~					0,130
2 x 1015				0,i00	
2 x IO Il&				0.i~5	0,200
3 x 10~15					0,220
3 x IO II*				0.182	
5 x 10~15					0,300
7 x 10~15				0.2-6	0,32 9
5 x IO II*		I 540		0.29~	
i x 1016				o.h00	0,391
7 x 1014				o,h00	
9 x 1014	12, 5				
1 x 10~15				0.588	0.453
1, 3 x iO 15					O,b-l
1.6 x 10~15				0.80o	0.5oo
1.8 x 10~15				0.900	0.522
2 x 10~15				1,000	0,525

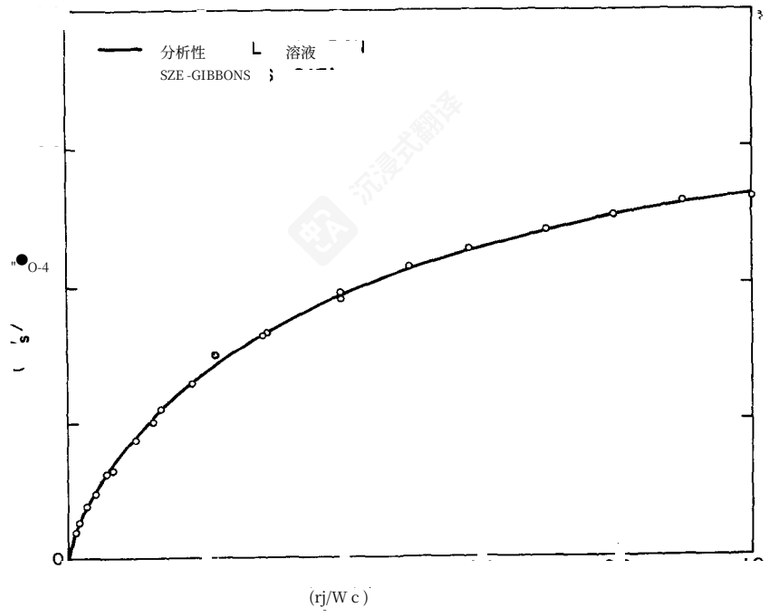

图3. 分析解中归一化击穿电压与球形结计算机求解结果的比较。

and

$$V = \frac{qN_B}{3\epsilon\epsilon_0}\left[\left(\frac{r_j^2 - r^2}{2}\right) + r_a^3\left(\frac{1}{r_j} - \frac{1}{r}\right)\right]. \quad (22)$$

As in the case of cylindrical junctions, the ionization is largely confined to small values of r near the metallurgical junction and the approximation

$$E = \frac{K}{r^2} \quad (23)$$

can be used instead in the ionization integral. Performing the integration from r_j to infinity as before gives the peak electric at breakdown for spherical junctions:

$$E_{pS} = \left(\frac{13}{Ar_j}\right)^{1/7}. \quad (24)$$

Normalizing to the corresponding parallel plane case gives

$$\frac{E_{pS}}{E_{pPP}} = \left(\frac{13}{8}\frac{W_c}{r_j}\right)^{1/7}. \quad (25)$$

Unlike the cylindrical case, no solutions for the peak electric fields in spherical junction are available for comparison.

Proceeding to the breakdown voltage of spherical junctions, a normalization to the parallel plane case gives

$$\frac{BV_S}{BV_{PP}} = \frac{2}{W_c E_{pPP}}\left[\frac{qN_B}{2\epsilon\epsilon_0} r_j^2 - E_{pS} r_j - \frac{qN_B}{2\epsilon\epsilon_0}\left(r_j^3 - \frac{3\epsilon\epsilon_0 r_j^2 E_{pS}}{qN_B}\right)^{2/3}\right] \quad (26)$$

which, with the application of (25), reduces to

$$\frac{BV_S}{BV_{PP}} = \left\{\left(\frac{r_j}{W_c}\right)^2 + 2.14\left(\frac{r_j}{W_c}\right)^{6/7} - \left[\left(\frac{r_j}{W_c}\right)^3 + 3\left(\frac{r_j}{W_c}\right)^{13/7}\right]^{2/3}\right\}. \quad (27)$$

This formulation for the breakdown voltage of spherical junctions is compared to the solutions obtained from Sze and Gibbons (Table 3) in Fig. 3. Agreement is once again extremely good over the range (r_j/W_c) from 0 to 1. As in the case of cylindrical junctions, this solution cannot be applied when the background doping exceeds 1×10^{16} cm^{-3} and when the ratio (r_j/W_c) exceeds unity.

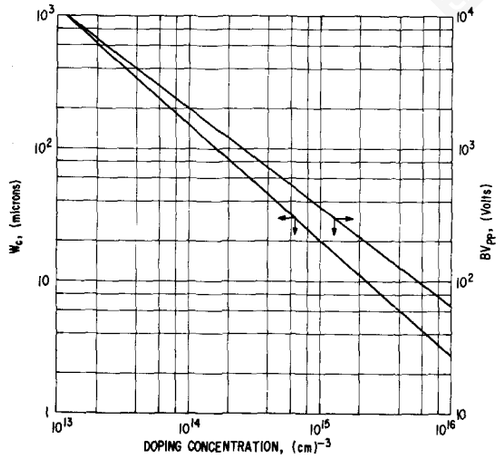

Fig. 4. Breakdown voltage and depletion layer width at breakdown for abrupt parallel plane junctions in silicon.

DISCUSSION AND CONCLUSIONS

It was shown in the earlier sections that the breakdown voltage of both cylindrical junctions and spherical junctions can be condensed into a single curve applicable to each case. This compact presentation replaces the multiplicity of curves that have been used in the past. However, to obtain the breakdown voltage of the curved junction, a calculation of the breakdown voltage (BV_{PP}) of the corresponding parallel plane case (same background doping) as well as the depletion layer width at

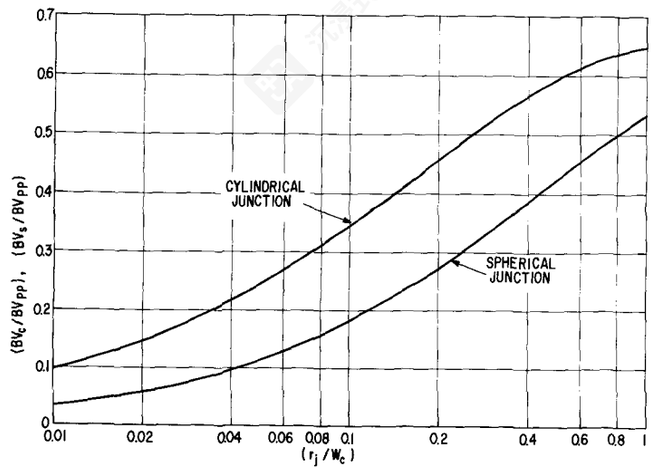

Fig. 5. Design curves for the determination of the breakdown voltage of abrupt cylindrical and spherical junctions in silicon.

得到

$$V = \frac{qN_B}{3\epsilon\epsilon_0}\left[\left(\frac{r_j^2 - r^2}{2}\right) + r_a^3\left(\frac{1}{r_j} - \frac{1}{r}\right)\right].$$

与圆柱形结的情况类似，电离主要局限于靠近冶金结的小r值附近，并且可以使用近似

$$E = \frac{K}{r^2}$$

在电离积分中可以代替使用。按照之前的方式从rj积分到无穷大，得到球形结击穿时的峰值电场：

$$E_{pS} = \left(\frac{13}{Ar_j}\right)^{1/7}.$$

与平行平面情况相比，球形结的峰值电场没有可用于比较的解。

$$\frac{E_{pS}}{E_{pPP}} = \left(\frac{13}{8}\frac{W_c}{r_j}\right)^{1/7}.$$

与圆柱形情况不同，球形结的峰值电场没有可用于比较的解。

接下来讨论球形结的击穿电压，对平行平面情况归一化后得到

$$\frac{BV_S}{BV_{PP}} = \frac{2}{W_c E_{pPP}}\left[\frac{qN_B}{2\epsilon\epsilon_0} r_j^2 - E_{pS} r_j - \frac{qN_B}{2\epsilon\epsilon_0}\left(r_j^3 - \frac{3\epsilon\epsilon_0 r_j^2 E_{pS}}{qN_B}\right)^{2/3}\right] \quad (26)$$

应用(25)式后，可简化为

$$\frac{BV_S}{BV_{PP}} = \left\{\left(\frac{r_j}{W_c}\right)^2 + 2.14\left(\frac{r_j}{W_c}\right)^{6/7} - \left[\left(\frac{r_j}{W_c}\right)^3 + 3\left(\frac{r_j}{W_c}\right)^{13/7}\right]^{2/3}\right\}.$$

球形结击穿电压的此公式与Sze和Gibbons（表3）得到的解在图3中进行比较。在(rj/W,)范围从0到1内，结果依然非常吻合。与圆柱形结的情况类似，当背景掺杂超过1×1016cm ~且 *(ri/W~)* 比值超过1时，此解不适用。

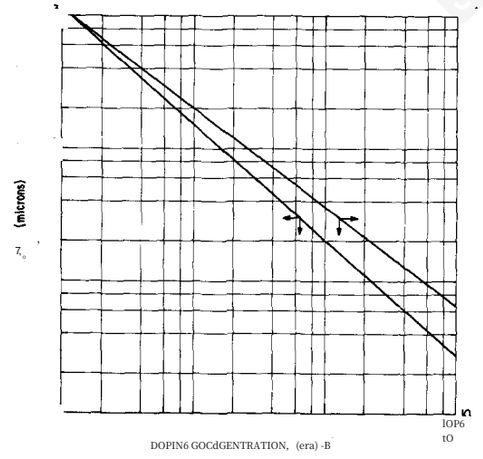

图4。硅中突变平行平面结的击穿电压和耗尽层宽度。

讨论与结论

在之前的章节中已经表明，圆柱形结和球形结的击穿电压可以被简化为适用于每种情况的单一曲线。这种简洁的表达方式取代了过去使用的多种曲线。然而，为了获得弯曲结的击穿电压，需要进行计算，包括对应平行平面情况（相同背景掺杂）的击穿电压（BVpp）以及耗尽层宽度

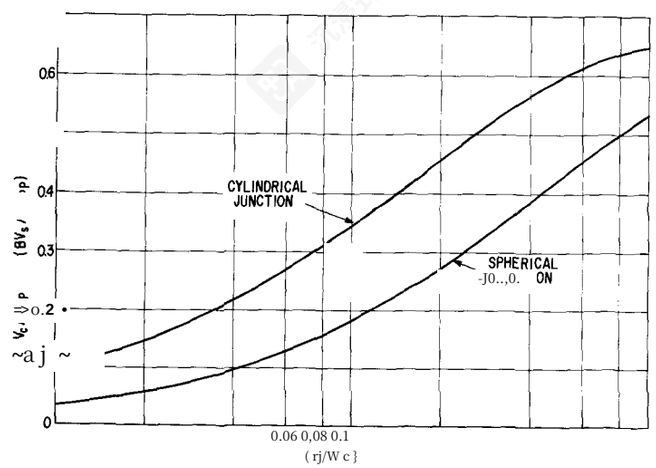

图5. 硅中陡峭圆柱形和球形结击穿电压确定的设计曲线。

breakdown (W_c) of the parallel plane case, must still be performed.

Figures 4 and 5 have been provided to facilitate these calculations, and comprise all the information necessary for determining the breakdown voltage of cylindrical and spherical junctions for silicon with background doping of less than 1×10^{16} cm^{-3}. Although Fig. 5 can only be used for the calculation of the breakdown voltages of junctions with a radius of curvature less than the depletion layer width at breakdown in the corresponding parallel plane case, most practical junctions used for the fabrication of devices fall into this category. This is, therefore, not a serious limitation to the solutions presented here.

Acknowledgements—This work was partly supported by Grant No. ENG75-01490 from the National Science Foundation. The authors would like to thank R. C. Rafun for assistance in manuscript preparation.

REFERENCES

1. S. M. Sze and G. Gibbons, *Solid-St. Electron.* **9**, 831 (1966).
2. O. Leistiko and A. S. Grove, *Solid-St. Electron.* **9**, 847 (1966).
3. D. V. Speeney and G. P. Carey, *Solid-St. Electron.* **10**, 177 (1967).
4. P. R. Wilson, *Proc. IEEE* **55**, 1483 (1967).
5. R. M. Warner, *Solid-St. Electron.* **15**, 1303 (1972).
6. D. A. Vincent, H. Rombeck, R. E. Thomas, R. M. Sirsi and A. R. Boothroyd, *Solid-St Electron.* **14**, 1193 (1971).
7. P. R. Wilson, *Solid-St. Electron.* **16**, 991 (1973).
8. D. P. Kennedy and R. R. O'Brien, *IBM J. Res. and Dev.* **10**, 213 (1966).
9. C. Bulucea *et al.*, *Solid-St. Electron.* **17**, 881 (1974).
10. V. A. K. Temple *et al.*, *IEEE-ED* **22**, 910 (1975).
11. S. M. Sze, *Physics of Semiconductor Devices*, Chap. 2. Wiley-Interscience, New York (1969).
12. C. A. Lee, R. A. Logan, R. L. Batdorf, J. J. Kleimack and W. Wiegmann, *Phys. Rev.* **134**, A761 (1964).
13. W. Fulop, *Solid-St. Electron.* **10**, 39 (1967).

击穿（W，）的平行平面情况，仍然必须执行。

图4和图5已提供以方便这些计算，并包含确定具有小于 1× 10-6 cm^3 背景掺杂的硅圆柱形和球形结击穿电压所需的所有信息。尽管图5只能用于计算曲率半径小于相应平行平面情况下击穿时耗尽层宽度的结的击穿电压，但大多数用于器件制造的实用结都属于此类。因此，这对这里提出的解决方案不是严重的限制。

致谢——这项工作部分得到了国家科学基金会 ENG75-01490 号资助。作者感谢 R. C. Rafun 在稿件准备方面的协助。

参考文献

1. S. M. Sze and G. Gibbons, *Solid-St. Electron.* **9**, 831 (1966).
2. O. Leistiko and A. S. Grove, *Solid-St. Electron.* **9**, 847 (1966).
3. D. V. Speeney and G. P. Carey, *Solid-St. Electron.* **10**, 177 (1967).
4. P. R. Wilson, *Proc. IEEE* **55**, 1483 (1967).
5. R. M. Warner, *Solid-St. Electron.* **15**, 1303 (1972).
6. D. A. Vincent, H. Rombeck, R. E. Thomas, R. M. Sirsi and A. R. Boothroyd, *Solid-St Electron.* **14**, 1193 (1971).
7. P. R. Wilson, *Solid-St. Electron.* **16**, 991 (1973).
8. D. P. Kennedy and R. R. O'Brien, *IBM J. Res. and Dev.* **10**, 213 (1966).
9. C. Bulucea *et al.*, *Solid-St. Electron.* **17**, 881 (1974).
10. V. A. K. Temple *et al.*, *IEEE-ED* **22**, 910 (1975).
11. S. M. Sze, *Physics of Semiconductor Devices*, Chap. 2. Wiley-Interscience, New York (1969).
12. C. A. Lee, R. A. Logan, R. L. Batdorf, J. J. Kleimack and W. Wiegmann, *Phys. Rev.* **134**, A761 (1964).
13. W. Fulop, *Solid-St. Electron.* **10**, 39 (1967).